Journal of Molecular Liquids 359 (2022) 119188

Contents lists available at ScienceDirect

Journal of Molecular Liquids

journal homepage: www.elsevier.com/locate/molliq

Structure, dynamics and ionic conductivities of ternary ionic liquid/lithium salt/DMSO mixtures

Pablo Martínez-Crespo [a,1], Martín Otero-Lema [a,1], Oscar Cabeza [b], Hadrián Montes-Campos [a,*], Luis M. Varela [a,**]

[a] Grupo de Nanomateriais, Fotónica e Materia Branda, Departamento de Física de Partículas, Facultade de Física and Instituto de Materiais (iMATUS), Universidade de Santiago de Compostela, Campus Vida s/n E-15782, Santiago de Compostela, Spain
[b] Facultade de Ciencias, Universidade da Coruña, Campus A Zapateira s/n E-15071, A Coruña, Spain

ARTICLE INFO

Article history:
Received 3 March 2022
Accepted 15 April 2022
Available online 28 April 2022

Keywords:
Ionic liquids
Conductivity
Structure
DMSO
Molecular dynamics simulations
Density functional theory

ABSTRACT

In this paper we report classical Molecular Dynamics and ab initio Density Functional Theory simulations of the structure and single particle dynamics of ternary mixtures of a protic (ethylammonium nitrate, EAN) and an aprotic (1-Ethyl-3-methylimidazolium tetrafluoroborate, $EMIMBF_4$) ionic liquid, lithium salts with common anion and a molecular cosolvent, dimethyl sulfoxide (DMSO). The coordination numbers and electrical conductivities of the different mixtures have been calculated throughout the whole concentration range, and the differences between mixtures with the protic and aprotic ionic liquids were analyzed. In both cases, the evolution of the electrical conductivity is seen to correlate well with the formation of mixed tetrahedral solvation complexes of lithium cations with ionic liquid anions and cosolvent molecules. The differences in the solvation and charge transport mechanisms in hydrogen bonded mixtures and those based in the aprotic ionic liquid are analyzed. Our conclusions indicate that the major feature behind the electrical conductivity of the ternary mixtures is the composition of the solvation shell of the metal cations in the mixtures and the rate at which anions in it are replaced by DMSO molecules.

1. Introduction

Electrochemical energy storage is crucial in the pursuit of a model for sustainable development due to its application in electric vehicles and as a support in devices for power generation from renewable energy sources. Mainly, lithium-ion batteries have fulfilled our energy storage needs since Sony first commercialized them in 1991. Nevertheless, their insufficient energy density and unsatisfying security standards, due to their reliance on liquid organic solvent-based electrolytes, are hindering the advancement of electric vehicles. As a consequence, it is imperative to find new electrolytes that enable safer and energy-denser battery chemistries.

Ionic liquids (ILs) are molten salts with their melting point lying below 100 °C. They are usually made up of a bulky organic cation and an inorganic anion, which handicaps crystal packing and keeps a low melting temperature. The large number of possible anion-cation combinations makes them highly tunable substances, which is interesting for the field of electrochemical energy storage, among others [1–3]. Moreover, the nonvolatility and nonflammable nature of ILs may enable safer and more stable batteries. IL-based electrolytes stand as an alternative due to remarkable features as high ionic conductivity, wide electrochemical stability windows and environmental friendliness. Alas, they are burdened by low Li^+ transference number and very high viscosity, negatively impacting ion transport properties. A remedy for this is the addition of organic solvents to reduce the coordination of Li^+ ions with the anions from the IL to enhance mobility and conductivity, as well as transport numbers [4]. For all these reasons, mixing ILs, solvents and metal salts is a promising strategy towards next generation batteries. Oldiges et al. [5] already followed this procedure in a molecular dynamics (MD) and experimental study for two salts: LiTFSI and $LiPF_6$. They dissolved these salts in several 1-butyl-1-methylpyrrolidinium bis(trifluoromethylsulfonyl) imide ($Py_{14}TFSI$) with ethylene carbonate and dimethyl carbonate mixtures, showing that a high IL concentration would impact negatively in transport and transference processes. Moreover, Li et al. [6] proved that this approach may also solve interfacial issues, mixing $Py_{13}TFSI$, dimethoxyethane, dioxolane and LiTFSI with

* Corresponding author.
** Corresponding author.
E-mail addresses: hadrian.montes@usc.es (H. Montes-Campos), luismiguel.varela@usc.es (L.M. Varela).
[1] Contributed equally to this work.

https://doi.org/10.1016/j.molliq.2022.119188
0167-7322/

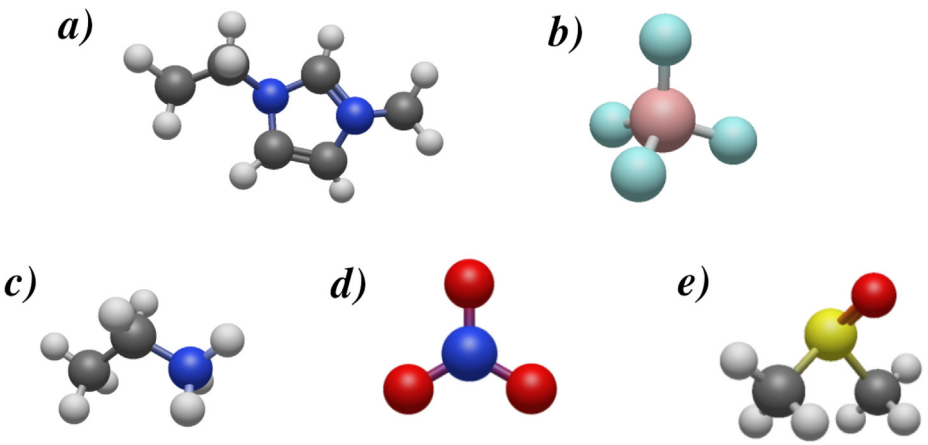

Fig. 1. 3D models of the molecules comprising the simulated substances. a) $[EMIM]^+$, b) BF_4^-, c) $[EA]^+$, d) NO_3^- and e) DMSO. White, grey, navy, light blue, pink, red and yellow correspond to H, C, N, B, F, O and S, respectively. Designed with Avogadro 1.93.0 [11,12].

regard to stabilizing the passivation of a lithium metal anode. Hence, tuning the concentration of the different components of the mixture is essential for achieving the appropriate transport properties of the electrolyte.

However, there is still a lack of understanding of the behaviour of these complex mixtures at the microscopic scale. For this, computer simulations are a valuable tool in this regard, since they provide us the capability of studying this kind of systems from the atomic scale. On the one hand, classical MD simulations enable the study of long trajectories of the molecules in electrolyte mixture. On the other hand, Density Functional Theory (DFT) computations may provide valuable information about their geometry and stability properties at the microscopic scale.

In this work, both types of simulations for mixtures of two different ILs [EMIM][BF_4], Fig. 1 a) and b) and EAN (Figs. 1 c) and d)) and a lithium salt with common anion have been performed, EAN being a protic IL and [EMIM][BF_4] being aprotic. As a molecular cosolvent we chose dimethyl sulfoxide (DMSO, Fig. 1 e)- a highly polar (μ=3.96 D) solvent with a wide electrochemical window (4.4 V) and miscible with water and organic solvents, quite often used in electrochemical devices [7–10]. The goal is to improve our current understanding of the evolution of the solvation shells of the Li^+ with the concentration of the cosolvent, and their effect on the conductivity, as well as to clarify the differences between protic and aprotic ILs in this context.

2. Methodology

In this work, several MD and DFT simulations were run for two different ionic liquids: EAN and [EMIM][BF_4]. In both cases, we studied the change in structural and dynamical properties with the addition of DMSO. Besides, ternary mixtures of IL + solvent with a lithium salt were analysed: $LiBF_4$ in the $EMIMBF_4$ mixture and $LiNO_3$ in the EAN one.

2.1. Molecular dynamics methods

Binary mixtures of IL + DMSO and ternary mixtures of the same systems with common-anion lithium salt were simulated using the Groningen Machine for Chemical Simulations (GROMACS) version 2019.5 [13]. The Optimized Potentials for Liquid Simulations in its all-atoms version (OPLS-AA) force field was employed [14,15]. Simulations were conducted across a whole range of DMSO concentration - from 0 % up to 100 % molar fraction of DMSO. The parameters for the simulation of the DMSO were obtained from Ref. [16], while the parameters for the ILs have been already reported in Ref. [17]. For the Li^+ cation the OPLS_404 atom model with a charge of $+1e$ was used, following the methodology presented in Ref. [18].

The process followed for simulating the binary and ternary mixtures was the same and can be divided in several steps. Firstly, simulation boxes were generated using PACKMOL [19], with a suitable number of molecules, which we will discuss later. Once the boxes were generated an energy minimization was carried out with GROMACS using a conjugate gradient algorithm with a 0.1 kJ $mol^{-1}nm^{-1}$ tolerance and an initial step of 0.01 nm. A steepest descent algorithm minimization was needed in some cases prior to conjugate gradient with the same tolerance and initial step. After that a 20 ns long stabilization in the NPT ensemble was performed. Finally, production runs were performed from the previously stationary-state starting points also in the NPT ensemble. These production runs were performed for 20 ns with a 1 fs timestep recording the positions of all atoms were recorded every 500 timesteps.

All the NPT simulations were performed with a pressure of 1 atm and a temperature of 298.15 K. The temperature was kept constant by a velocity re-scale algorithm with a stochastic term [20] with a 0.1 ps coupling constant. Moreover, an isotropic Parrinello-Rahman barostat, with 1 ps coupling time as using for keeping the pressure constant. Coulomb interaction was computed by smooth Particle-Mesh Ewald electrostatics [21], i.e., real space positions are used for particles within a cut-off radius and Fourier space is employed for the rest. Real space cut-off radius was 1.1 nm, whereas Fourier grid spacing was 0.12 nm with cubic interpolation. Finally, van der Waals forces were considered with long range dispersion corrections for the energy and the pressure and a 1.1 nm cut-off radius.

The total number of molecules of the mixture was fixed to 1000 in the majority of the simulations, with the exception of the simulations of those for EAN + DMSO binary system at DMSO concentrations of 95% or more, where the total number of molecules had to be scaled upwards in order to obtain reliable statistics in this low IL concentration regime. The precise number of molecules of each species for the different concentrations can be found in the table S1 of the supplementary information. For ternary configurations, 75 salt molecules were always used. The exact number of molecules of each species as a function of solvent concentration can be found in Table S2. Box sizes were varied during the simulations to properly fit the different concentrations.

Table 1
Solvent descriptors for the SMD model implicit solvent DFT simulations in Gaussian. All descriptors are dimensionless except γ, which has units of cal mol^{-1} Å^{-2}. Abraham's hydrogen bonding parameters for the ionic liquids were computed according to Ref. [26]. DMSO values are taken form Ref. [32].

	DMSO	EAN	$EMIMBF_4$
n^2	2.185371	2.1115 [29]	1.987536 [26]
$\Sigma\alpha_2^H$	0.0	0.35473	0.29326
$\Sigma\beta_2^H$	0.88	0.371348	0.248588
γ	61.78	69.28886 [30]	78.3 [26]
ε	46.826	28.73 [31]	12.8 [26]
ϕ	0.0	0.0	0.2308 [26]
ψ	0.0	0.0	0.3077 [26]

n^2 square of index of refraction at optical frequencies at 298 K.
$\Sigma\alpha_2^H$ Abraham's hydrogen bond acidity.
$\Sigma\beta_2^H$ Abraham's hydrogen bond basicity.
γ Macroscopic surface tension at a liquid–air interface at 298 K in cal mol^{-1} Å^{-2}.
ε Dielectric constant (relative permittivity) at 298 K.
ϕ Aromaticity: fraction of non-hydrogenic solvent atoms that are aromatic carbon atoms.
ψ Electronegative halogenicity: fraction of non-hydroge-nic solvent atoms that are F, Cl, or Br.

2.2. Density functional theory methods

Equilibrium geometries of several Li compounds were computed with Gaussian 16 [22] (displayed in Fig. 5). The calculations were performed using the B3LYP exchange and correlation hybrid functional [23,24] and the $6-311g(d,p)$ basis set [25]. In order to account for the effect of the solvent - and therefore achieve more reliable results - implicit solvent simulations were performed. SMD model [26] was used for the implicit solvents with the parameters shown in Table 1.

Values of Abraham's hydrogen bond acidity and basicity, $\Sigma\alpha_2^H$ and $\Sigma\beta_2^H$, for the ionic liquids were computed according to the expressions specified in Ref. [26]:

$$\Sigma\alpha_2^H = 0.4098\alpha + 0.0064, \quad (1a)$$

$$\Sigma\beta_2^H = 0.6138\beta + 0.089, \quad (1b)$$

where α and β are the Kamlet-Taft hydrogen bond acidity and basicity parameters of the corresponding ionic liquid. For [EMIM][BF_4], $\alpha = 0.70$ and $\beta = 0.26$ [27]. For EAN, $\alpha = 0.85$ and $\beta = 0.46$ [28].

3. Results and discussion

3.1. Structural properties

In order to analyze the microscopical structure of the different mixtures, the radial distribution functions (RDFs) were calculated for all four systems with MD simulations. From the RDFs, the cumulative radial distribution functions (CRDFs) were also computed in order to evaluate the different coordination numbers. These functions can be obtained from the production runs as:

$$RDF_{ab}(r) = \frac{V}{N_a N_b} \sum_{i=1}^{N_a} \sum_{j=1}^{N_b} \left\langle \delta\left(\left|\mathbf{r_i} - \mathbf{r_j}\right| - r\right)\right\rangle, \quad (2)$$

$$\mathrm{CRDF}_{ab}(r) = \frac{N_b}{V} \int_0^r 4\pi(r\prime)^2 g_{ab}(r\prime)dr\prime, \quad (3)$$

respectively. From the CRDF, the coordination number (CN) of b species surrounding a can be calculated as $\mathrm{CRDF}_{ab}(r_0)$, where r_0 corresponds to the distance of the first solvation shell of a and can be estimated as the position of the first minima of the RDF. For the RDF calculations, different references were used to compute the distances between the different molecules: the oxygen atom of the DMSO molecules; the nitrogen atom of $[NO_3]^-$; the nitrogen atom of $[EA]^+$; the boron atom of $[BF_4]^-$ and the center of the aromatic ring of $[EMIM]^+$.

The analysis of the RDF for the binary mixtures (Fig. 2) shows a similar general behaviour for both ILs. The structure of the pure IL does not seem to be greatly modified when DMSO is added to the system and no changes in the positions of the peaks are found. Both ILs show a stronger interaction between the cations and the DMSO than between the anions and the DMSO. This effect is the opposite to what is found when EAN is mixed with alcohols [33], but it is in line with experimental results of EAN-DMSO mixtures which suggest a very strong correlation between $[EA]^+$ cations and DMSO [34]. Moreover, these results also match the findings for a different imidazolium-based IL, [BMIM][TFO] mixed with DMSO and ethyleneglycol, which found a preferential interaction between the molecular solvent and the cation when the latter has hydrogen-bond acceptor groups and with the anion when it has donor groups [35]. This effect is enhanced - as may be seen in Fig. 2 - in the EAN mixtures due to the ability of the cation to form hydrogen bonds with DMSO.

Regarding the ternary mixtures, we analyzed the salt-IL and salt-DMSO RDFs for the simulations with both ILs, which are represented in Fig. 3. If we look at the salt-anion distribution (on the top row), we can see that their evolution is clearly different. The distribution for the EAN mixtures (left column) displays two peaks on the first solvation shell, as already observed by Méndez-Morales et al. [36]. These peaks represent a bidentate coordination (the closest one) and a monodentate coordination (the second one). We can see that as the concentration of DMSO increases, the height of both peaks also increases. This suggest that the stability of the Li-$[NO_3]^-$ complexes is very high and that DMSO molecules cannot easily replace the role of $[NO_3]^-$ anions in the coordination complexes. Moreover, the relative heights of these peaks change throughout the DMSO molar fraction spectrum, i.e. the second peak is higher than the first one at low DMSO concentrations, but the first one is predominant at high concentrations of the molecular solvent. This represents a change in coordination preference, from a monodentate coordination at low DMSO concentrations to a bidentate coordination at high DMSO concentrations, which may be induced by the presence of more DMSO molecules in the first solvation shell at high DMSO concentrations. On the other hand, Li-anion distribution for the [EMIM][BF_4] mixtures shows a single peak, which has the opposite trend than that of EAN mixtures and it decreases as the concentration of DMSO molecules in the mixture is increased (except for a slight growth from 80 to 85 and 90%).

Interestingly, the RDFs of the Li^+ ions around DMSO molecules show a very different behaviour depending on the nature of the IL they are solvated into. While DMSO molecules show a very intense interaction with the Li^+ ions at high concentration of [EMIM][BF_4] and it decreases in magnitude as the amount of DMSO increases, the mixtures with EAN show a much weaker interaction between Li^+ and DMSO which becomes stronger as the amount of DMSO increases. This difference seems to be caused by the strong interaction that the binary mixtures show between the $[EA]^+$ ions and the DMSO molecules. This, in turn, hinders the interaction between the oxygen atom of the DMSO and the Li^+ ions. These remarks imply that DMSO can easily replace the BF_4^- ions in the Li^+-$[BF_4]^-$ complexes, but it is more difficult for them to replace the $[NO_3]^-$ of Li^+-$[NO_3]^-$, due to the preferential interaction of the DMSO molecules with the $[EA]^+$ ions of the IL.

From the RDFs of Figs. 2, 3 we estimated the value of r_0 to calculate CNs in the first solvation shell, which values can be found in Table 2. The CNs for the binary mixtures are represented in Fig. 4 and, as can be seen there, both ILs show a progressive substitution of molecules in the first solvation shell of the cation. However, this

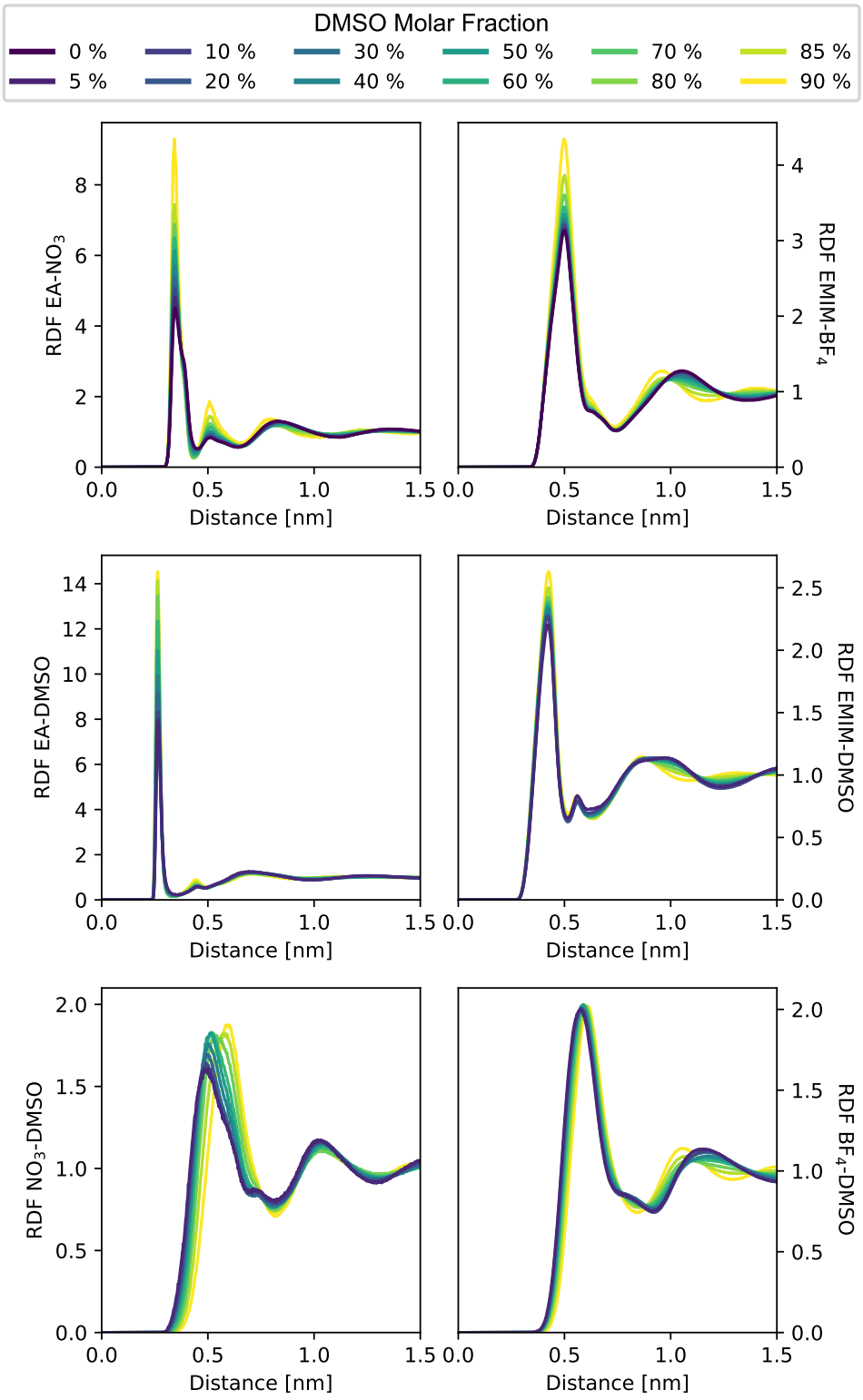

Fig. 2. Radial distribution functions for the binary mixtures (left EAN + DMSO, right [EMIM][BF_4]+DMSO. The following RDFs are represented from top to bottom: anion-cation, cation-DMSO, anion-DMSO.

substitution happens at different rates depending on the IL, with the substitution around $[EA]^+$ cations being a little faster than around $[EMIM]^+$ cations. The coordination numbers for the $[EA]^+$ can be easily explained by the formation of hydrogen bonds between the cation and the molecular solvent, as previously discussed. Moreover, the values obtained with this analysis are in agreement with those reported by Russina et al. [34].

Regarding the ternary mixtures, their CNs are represented in Fig. 5. The CNs show that the addition of the Li^+ salts does not impact the IL structure, at least in the small quantities introduced for these simulations. The Li^+-anion and Li^+-solvent CNs are also of

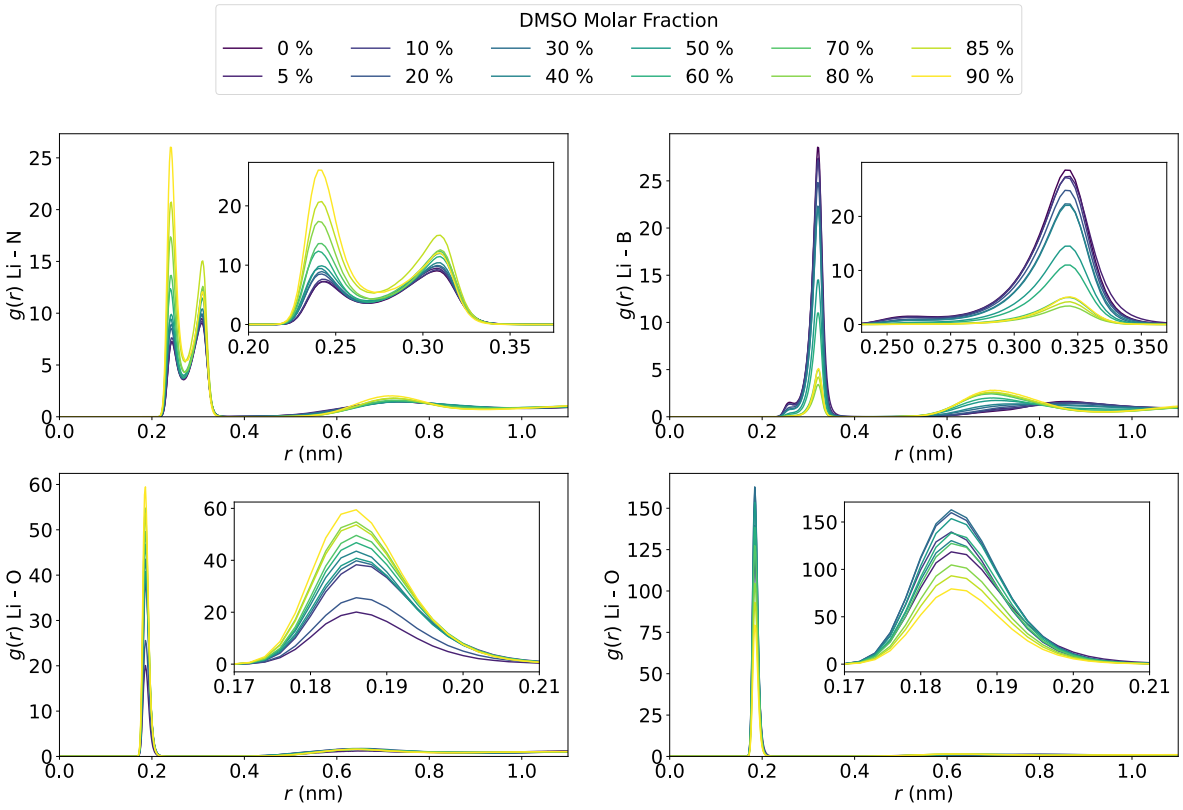

Fig. 3. Radial distribution functions computed for the structural analysis of the ternary mixtures. Left column is for EAN + DMSO + $LiNO_3$, right column is for [EMIM][BF_4] +DMSO + $LiBF_4$. The O atom in Li-O RDFs belongs to DMSO molecules. Legend is common for the four plots. The reference atoms chosen for the computation are shown in the *y* axis.

Table 2
Coordination distances for binary and ternary mixtures of EAN (top) and [EMIM][BF_4] (bottom).

	$[EA]^+$	NO_3^-	DMSO	Li^+
$[EA]^+$	-	4.5 Å	3.5 Å	-
NO_3^-	4.5 Å	-	8 Å	3.5 Å
DMSO	3.5 Å	8 Å	-	3.5 Å
Li^+	-	3.5 Å	3.5 Å	-
	$[EMIM]^+$	BF_4^-	DMSO	Li^+
$[EMIM]^+$	-	7.5 Å	8.5 Å	-
$[BF_4]^-$	7.5 Å	-	8.5 Å	3.8 Å
DMSO	8.5 Å	8.5 Å	-	3.5 Å
Li^+	-	3.8 Å	3.5 Å	-

great interest and they reveal deep changes in the structure of the Li^+ first coordination shell. The mixtures with both ILs show, in general terms, the same picture for the Li^+ complexes, starting with a $[LiA_4]_3^-$ tetrahedral configuration when no DMSO is present and progressively turning into $[LiDMSO_4]^+$ as the concentration of DMSO increases. Moreover, the Li^+ complexes in both system present a 1 to 1 substitution, where the anions are progressively substituted by DMSO molecules, but preserving at all times the tetrahedral coordination. However, just like in the binary mixtures, the rate at which this happens is very different between both systems. As can be seen in Fig. 5, the replacement of anions with DMSO molecules is much slower in the EAN mixtures, specifically, the tipping point at which there are more DMSO molecules than IL anions happens at higher DMSO concentration. It is also very interesting that, despite the smaller size of the Li^+ ions compared to the EA^+ ions, their coordination with the anions of the IL is higher for Li^+. Both effects can be explained by the already mentioned hydrogen bonding between the $[EA]^+$ and the DMSO, which prevents the substitution of anions in the Li^+ complexes.

3.2. Conductivity analysis

For all systems, electrical conductivity was calculated using the Nernst-Einstein equation

$$\sigma = \frac{e^2}{Vk_BT}\sum_i N_i z_i D_i, \tag{4}$$

where N_i is the number of ions of each species, z_i their respective valence, and D_i the corresponding diffusion coefficient. This expression is in principle only valid when the concentration of charged species is low, as it neglects possible correlations between the ions [37]. However, it has been proven to accurately predict conductivity values of concentrated mixtures due to cancellations in the correlation among species [38]. For this reason, we will use Eq. (4) throughout the whole concentration range. Diffusion coefficients were obtained with the velocity autocorrelation function (VACF) of each charged species, given by

$$\mathrm{VACF}_i(t) = \langle \boldsymbol{v_i}(t+t_0)\cdot \boldsymbol{v_i}(t_0),\rangle \tag{5}$$

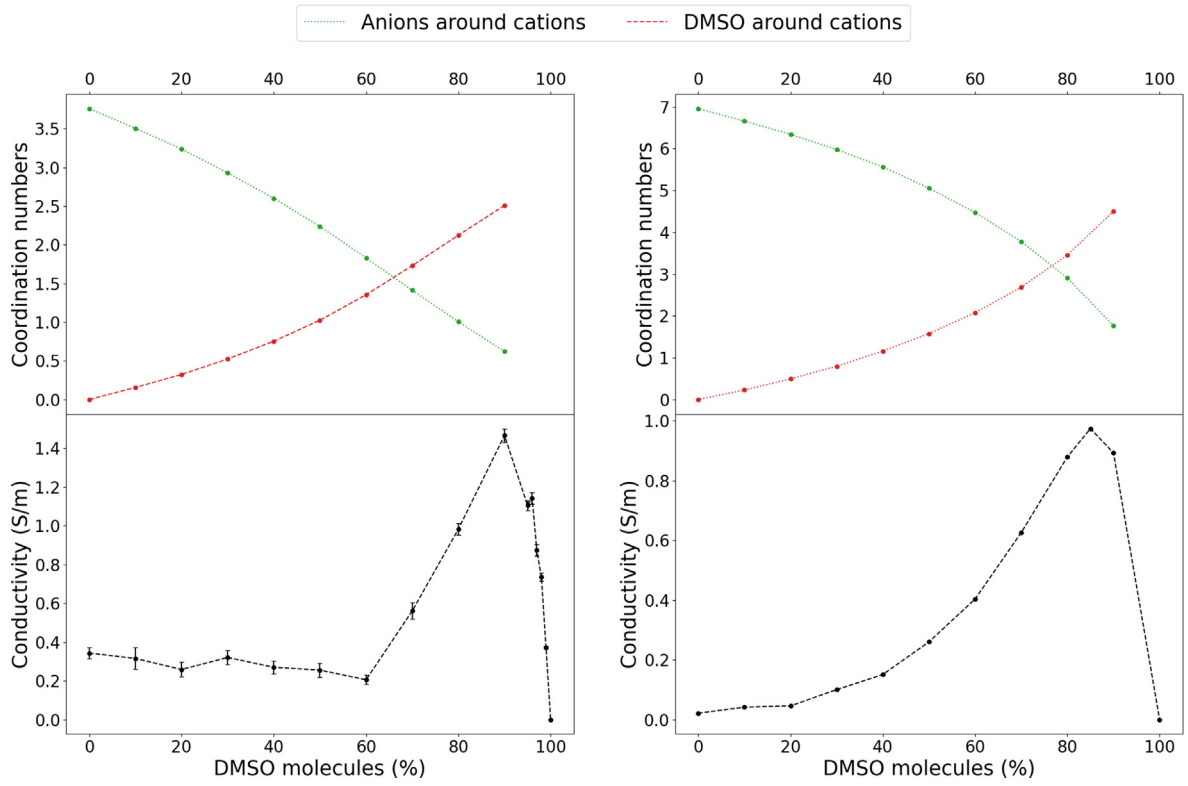

Fig. 4. Conductivity and anion-cation coordination number of IL + DMSO mixtures. The left graphs represent the results from the EAN mixtures, and the right ones depict the [EMIM][BF_4] ones. The coordination represented in the top row is the average number of solvent molecules around a cation (red dashed line) and the average number of anions around a cation (green dotted line). It can be clearly seen how solvent molecules gradually replace anions in the cation's solvation shell as DMSO rises. It is also clear that the total coordination around cations is kept constant through the whole concentration range, taking a value of around 3.5 for EAN and 7 for [EMIM][BF_4].

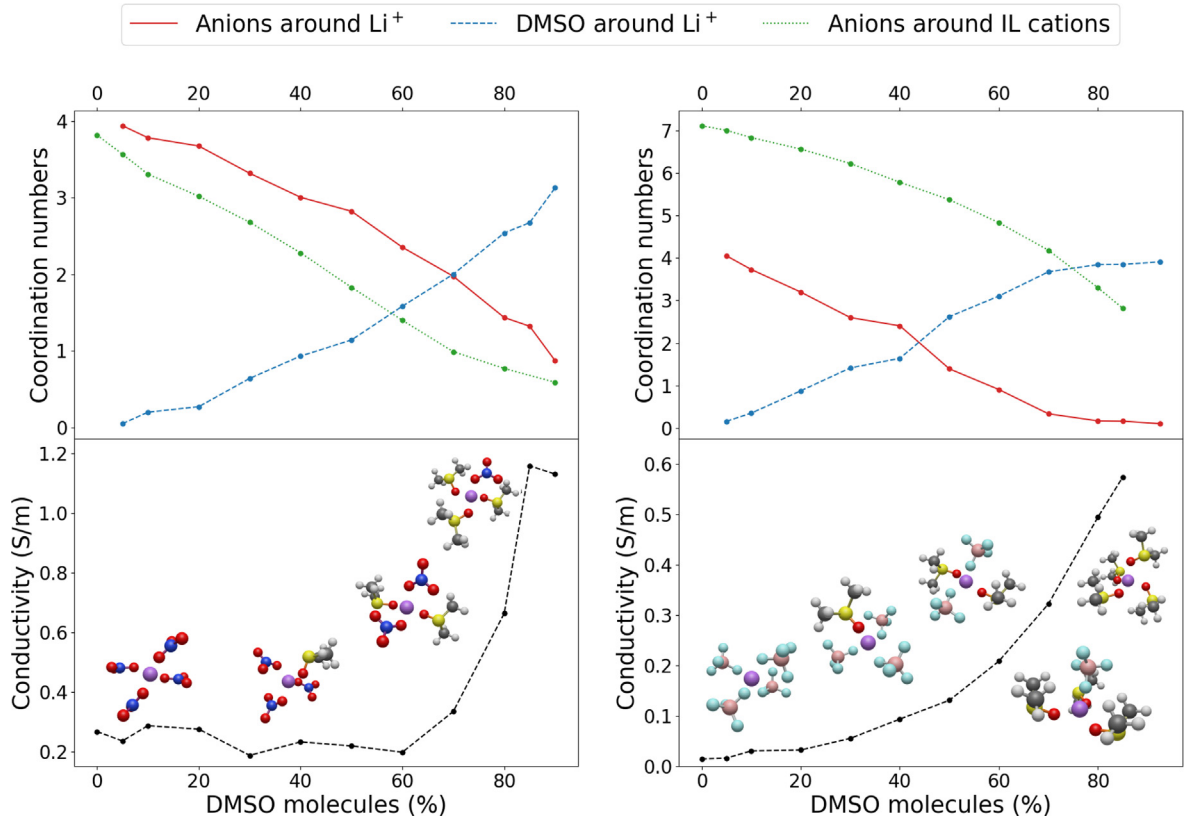

Fig. 5. Conductivity and coordination numbers for EAN (left) and [EMIM][BF_4] (right) mixtures. For the coordination, we display the average number of anions around Li^+ (red solid lines), solvent molecules around Li^+ (blue dashed lines) and anions around cations (green dotted lines). The various Li^+ solvation complexes obtained from DFT calculations are displayed as they begin to appear in the mixture.

where the brackets entail averaging over all ions of the i-th species, and over possible time origins t_0. This VACFs were computed from additional production runs in the NPT ensemble, simulating the systems for a total of 250 ps and recording the velocities at each step in order to ensure accurate statistics. From these correlation functions the diffusion coefficients can be calculated using the well-known Green–Kubo relation:

$$D_i = \frac{1}{3}\int_0^{\infty} \mathrm{VACF}_i(t)dt, \tag{6}$$

where the integral was performed numerically by calculating the cumulative integral and averaging its values once it has begun oscillating around a definite value, which happened after 50 ps. In order to estimate the uncertainty of the values, the remaining of the VACF was divided into 10 fragments and the variance of the mean in each fragment was used.

Once diffusion coefficients were determined, conductivities for all systems were calculated using Eq. (4), and the results are shown in Figs. 4 and 5 for the binary and ternary mixtures respectively. In both binary mixtures, the usual dome-like shape of the conductivity can be appreciated [39], reflecting the competition between the two driving forces of the conductivity: i) the number of charge carriers, which decreases as DMSO concentration rises; and ii) the mobility of charge carriers, which increases with DMSO concentration. This is due to the fact that, as the number of charge carriers decreases, so it does the strength of the electrostatic interaction in the IL, accordingly, thus increasing the diffusion coefficient. There is, however, a clear difference in the behaviour of the EAN and [EMIM][BF_4] mixtures. While the latter show a gradual increase in conductivity as DMSO is added to the pure IL, the mixtures with EAN show a sort of plateau at low DMSO concentrations, where the conductivity remains almost constant. This plateau finishes once a 70% molar fraction of DMSO is reached. This concentration is the same where the cation of the IL starts to have more DMSO in its first solvation shell than NO_3. This suggests that the hydrogen bond network that holds the EAN together is so severely impacted by the presence of DMSO (which can only form 1 hydrogen bond per molecule) once this concentration is reached that the system loses its rigidity.

The same competition is clearly reflected in the case of ternary mixtures, too. In these, highly electropositive Li^+ ions strongly attract the anion molecules of the ILs. This results in a mobility - and thus conductivity - downturn relative to the binary mixtures. Moreover, the different behaviours in the Li^+ solvation shell substitutions of each mixture seem to affect the corresponding curves of conductivity. EAN mixture shows greater aversion to change $[NO_3]^-$ for DMSO, due to the EA_+-DMSO hydrogen bonding, as reflected in its less steep CN curve in comparison to the [EMIM][BF_4] mixture. As a consequence, conductivity of EAN mixture shows a fast growth when the DMSO CN is greater than 2. Mean-

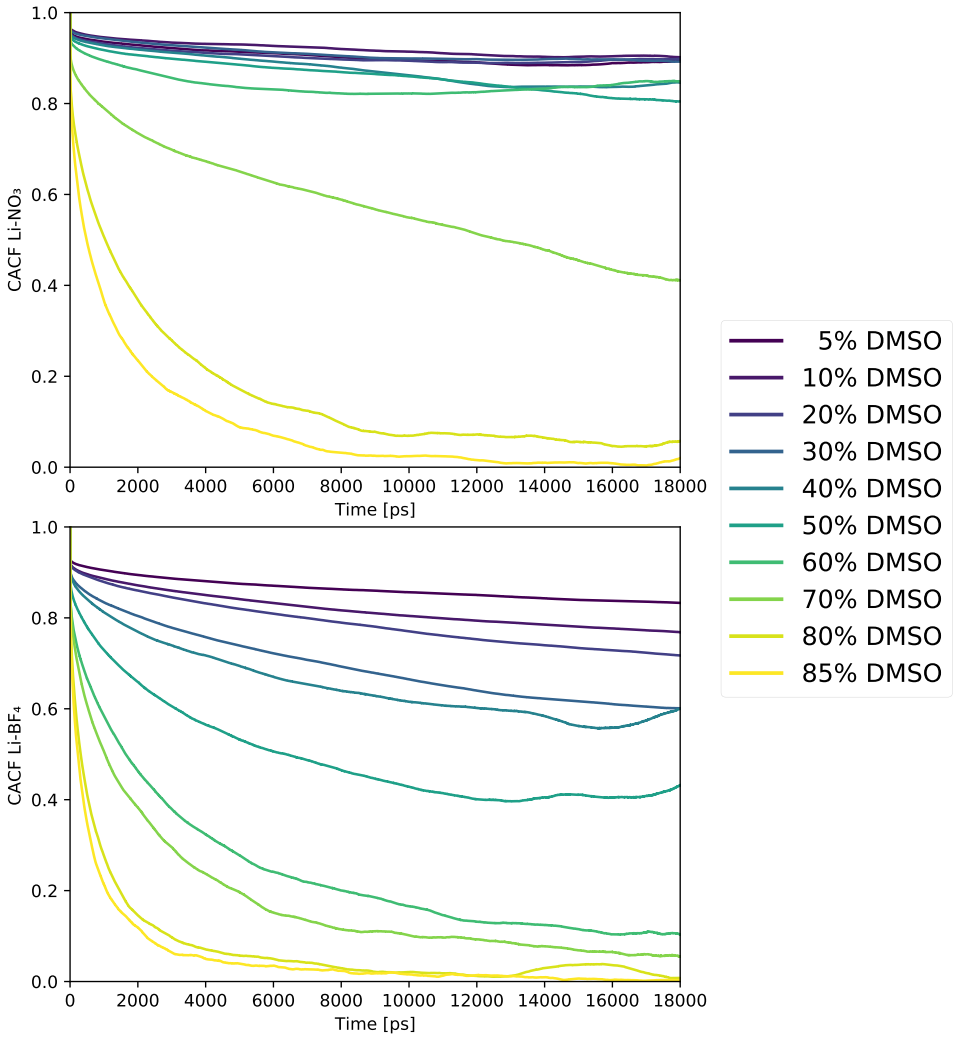

Fig. 6. Cage autocorrelation functions for EAN (top) and [EMIM][BF_4] (bottom).

while, the more gradual change in the CNs for the [EMIM][BF_4] mixture results in a slower growth of the conductivity.

On the other hand, whereas DMSO molecules comprise the whole Li^+ solvation shell at high solvent concentrations for the [EMIM][BF_4] mixture, at least one $[NO_3]^-$ anion is kept even for the less concentrated EAN mixtures. This may explain the final downturn in the conductivity of the latter, which would come from the decrease in mobility that takes due to the stronger interaction between the Li^+ and the NO_3^- compared to BF^{4-} (as can be seen in Fig. 3. For the [EMIM][BF_4] mixture, the solvation shell of Li^+ at high DMSO concentration is formed almost exclusively by solvent molecules. Consequently, a very fast increase in conductivity was obtained for the 925 DMSO + 75 $LiBF_4$ mixture, which reached $\sigma = 4.5874 \pm 0.0014$ S/m. Therefore, a direct relation between the composition of the Li^+ cations solvation shell and conductivity growth must exist.

To further study the robustness of the solvation structures that surround Li^+ cations in both mixtures, we computed the cage autocorrelation functions (CACF) of those ions

$$\mathrm{CACF}_{\mathrm{Li}^+-a}(t) = \frac{\langle \theta_a(t)\theta_a(0)\rangle}{\langle \theta_a^2(0)\rangle}, \tag{7}$$

where θ_a is a function that takes a value of 1 if the species a is in the first solvation shell of Li^+ cations and 0 otherwise. These CACFs take a value of 1 at $t = 0$, and then start decaying when the solvation complexes begin to break. Fig. 6 displays the CACFs for both ILs, taking the anion as the a species. It can be seen that the stability of the complexes as function of the DMSO concentration is completely different for each IL. While in the [EMIM][BF_4] mixture the cages become gradually feebler as solvent concentration rises, in the EAN systems this change from highly resilient cages with a high lifespan to short-lived solvation structures is much more abrupt, with a sudden change around 70 % DMSO concentration. CNs of anions and solvent molecules around Li^+ ions become equal at this concentration and the conductivity begins to increase (see Fig. 5), which again confirms that the microscopic structure of the Li^+ solvation complexes plays a key role in the conductivity of the system. In the case of [EMIM][BF_4], the smooth behaviour of the conductivity curve reflects the gradual changes in the CACFs for these systems. This analysis reveals that the hopping of Li^+ ions between adjacent solvation complexes does indeed play a key role in the conductivity of the mixture, and as such the analysis of the structure of the molecular cages can be of interest when studying it [39,40].

4. Conclusions

We simulated the structure and single-particle dynamics of ternary mixtures of ILs with lithium salts and DMSO for a protic (EAN) and an aprotic ([EMIM][BF_4]) IL. The structure and single-particle dynamics of the mixtures were analyzed by means of radial distribution functions, coordination numbers, velocity autocorrelation functions and cage autocorrelation functions. The RDFs clearly indicate that a replacement of anions A^- by DMSO molecules in the first solvation shell of Li^+ takes place as the concentration of this molecular solvent increases, giving rise to mixed tetrahedral solvation complexes whose structure was optimized by means of implicit solvent DFT simulations. Notwithstanding, the replacement rate is quite different for the protic and the aprotic IL. In the former case, the capability of the cations of the IL to form hydrogen bonds with the DMSO prevents the replacement on anions with DMSO in the Li-anion complexes. Moreover, the hydrogen bond network seems to further stabilize the microscopic structure Li-anion complexes. These effects dominate up to a 60% molar concentration of DMSO and are followed by an abrupt increase in conductivity as DMSO molecules outnumber IL anions in the first solvation shell of Li^+. Note that this capability of forming hydrogen bonds is a common characteristic of protic ILs. Therefore, one will expect a similar slow growth of the conductivity for most protic ILs with a molecular solvent which is a hydrogen bond acceptor. Alternatively, the structure and conductivity of the mixtures with aprotic IL undergo a more gradual variation with the concentration of DMSO, with DMSO molecules dominating in the first shell above 40% DMSO concentration. As proved by the cage correlation functions, when DMSO outnumbers anions in the first solvation shell of the salt cations the stability of complexes steeply decreases, and a large increase in conductivity is registered, suggesting that the solvation of the salt is the major phenomenon behind the charge transport in the mixture.

Declaration of Competing Interest

The authors declare that they have no known competing financial interests or personal relationships that could have appeared to influence the work reported in this paper.

Acknowledgements

The financial support of the Spanish Ministry of Economy and Competitiveness (Projects MAT2017-89239-C2-1-P, MAT2017-89239-C2-2-P) is gratefully acknowledged. Moreover, this work was funded by the Xunta de Galicia (ED431E 2018/08 and GRC 369 ED431C 2020/10). All these research projects were partially supported by FEDER. H. M-C. thanks the USC for his "Convocatoria de Recualificación del Sistema Universitario Español-Margarita Salas" postdoc grant under the "Plan de Recuperación, Transformación y Resiliencia" program funded by the Spanish Ministry of Universities with European Union's NextGenerationEU funds.

Appendix A. Supplementary data

Supplementary data associated with this article can be found, in the online version, at https://doi.org/10.1016/j.molliq.2022.119188.

References

[1] E. Jónsson, Ionic liquids as electrolytes for energy storage applications – A modelling perspective, Energy Storage Mater. 25 (2020) 827–835, https://doi.org/10.1016/j.ensm.2019.08.030.
[2] M. Galinski, A. Lewandowski, I. St, Ionic liquids as electrolytes, Electrochim. Acta 51 (2006) 5567–5580, https://doi.org/10.1016/j.electacta.2006.03.016.
[3] A. Lewandowski, A. Swiderska-Mocek, Ionic liquids as electrolytes for Li-ion batteries—An overview of electrochemical studies, J. Power Sources 194 (2009) 601–609, https://doi.org/10.1016/j.jpowsour.2009.06.089.
[4] G.H. Lane, A.S. Best, D.R. MacFarlane, M. Forsyth, P.M. Bayley, A.F. Hollenkamp, The electrochemistry of lithium in ionic liquid/organic diluent mixtures, Electrochim. Acta 55 (2010) 8947–8952, https://doi.org/10.1016/j.electacta.2010.08.023.
[5] K. Oldiges, D. Diddens, M. Ebrahiminia, J.B. Hooper, I. Cekic-Laskovic, A. Heuer, D. Bedrov, M. Winter, G. Brunklaus, Understanding transport mechanisms in ionic liquid/carbonate solvent electrolyte blends, Phys. Chem. Chem. Phys. 20 (2018) 16579–16591, https://doi.org/10.1039/c8cp01485j.
[6] N.-W. Li, Y.-X. Yin, J.-Y. Li, C.-H. Zhang, Y.-G. Guo, Passivation of Lithium Metal Anode via Hybrid Ionic Liquid Electrolyte toward Stable Li Plating/Stripping, Adv. Sci. 4 (2017) 2–7, https://doi.org/10.1002/advs.201600400.
[7] K. Pranay Reddy, P. Fischer, M. Marinaro, M. Wohlfahrt-Mehrens, Improved Li–Metal Cycling Performance in High Concentrated Electrolytes for Li-O_2 Batteries, ChemElectroChem 5 (2018) 2758–2766, https://doi.org/10.1002/celc.201800686.
[8] A. Khan, C. Zhao, Enhanced performance in mixture DMSO/ionic liquid electrolytes: Toward rechargeable Li-O_2 batteries, Electrochem. Commun. 49 (2014) 1–4, https://doi.org/10.1016/j.elecom.2014.09.014.

[9] M. Wang, X. Dong, I.C. Escobar, Y.-T. Cheng, Lithium Ion Battery Electrodes Made Using Dimethyl Sulfoxide (DMSO)—A Green Solvent, ACS Sustain. Chem. Eng. 8 (2020) 11046–11051, https://doi.org/10.1021/acssuschemeng.0c02884.
[10] M.A. Schroeder, N. Kumar, A.J. Pearse, C. Liu, S.B. Lee, G.W. Rubloff, K. Leung, M. Noked, DMSO–Li_2O_2 interface in the rechargeable Li–O_2 battery cathode: theoretical and experimental perspectives on stability, ACS Appl. Mater. Interfaces 7 (2015) 11402–11411, https://doi.org/10.1021/acsami.5b01969.
[11] M.D. Hanwell, D.E. Curtis, D.C. Lonie, T. Vandermeersch, E. Zurek, G.R. Hutchison, Avogadro: an advanced semantic chemical editor, visualization, and analysis platform, J. Cheminformat. 4 (2012) 17, https://doi.org/10.1186/1758-2946-4-17.
[12] Avogadro: an open-source molecular builder and visualization tool. version 1.93.0,://avogadro.cc, 2018.
[13] M. J. Abraham, D. van der Spoel, E. Lindahl, B. Hess, the GROMACS development team, GROMACS User Manual version 2019, http://www.gromacs.org.
[14] W.L. Jorgensen, D.S. Maxwell, J. Tirado-Rives, Development and Testing of the OPLS All-Atom Force Field on Conformational Energetics and Properties of Organic Liquids, J. Am. Chem. Soc. 118 (1996) 11225–11236, https://doi.org/10.1021/ja9621760.
[15] W.L. Jorgensen, J. Tirado-Rives, The OPLS [optimized potentials for liquid simulations] potential functions for proteins, energy minimizations for crystals of cyclic peptides and crambin, J. Am. Chem. Soc. 110 (1988) 1657–1666, https://doi.org/10.1021/ja00214a001.
[16] M.L. Strader, S.E. Feller, A flexible all-atom model of dimethyl sulfoxide for molecular dynamics simulations, J. Phys. Chem. A 106 (2002) 1074–1080, https://doi.org/10.1021/jp013658n.
[17] H. Montes-Campos, T. Mendez-Morales, J.M. Otero-Mato, O. Cabeza, L.J. Gallego, E. Lomba, L.M. Varela, Ionic liquids nanoconfined in zeolite-templated carbon: A computational study, J. Mol. Liq. 318 (2020) 114264, https://doi.org/10.1016/j.molliq.2020.114264.
[18] H. Montes-Campos, J.M. Otero-Mato, R.C. Longo, O. Cabeza, L.J. Gallego, L.M. Varela, Mixtures of lithium salts and ionic liquids at defected graphene walls, J. Mol. Liq. 289 (2019) 111083, https://doi.org/10.1016/j.molliq.2019.111083.
[19] A.-R. Allouche, Software News and Updates Gabedit — A Graphical User Interface for Computational Chemistry Softwares, J. Comput. Chem. 32 (2012) 174–182, https://doi.org/10.1002/jcc.21600.
[20] G. Bussi, D. Donadio, M. Parrinello, Canonical sampling through velocity rescaling, J. Chem. Phys. 126 (2007) 014101, https://doi.org/10.1063/1.2408420.
[21] U. Essmann, L. Perera, M.L. Berkowitz, T. Darden, H. Lee, L.G. Pedersen, A smooth particle mesh ewald method, J. Chem. Phys. 103 (1995) 8577–8593, https://doi.org/10.1063/1.470117.
[22] M. J. Frisch, et al., Gaussian16, 2016. Gaussian Inc. Wallingford CT.
[23] A.D. Becke, Density-functional exchange-energy approximation with correct asymptotic behavior, Phys. Rev. A 38 (1988) 3098–3100, https://doi.org/10.1103/PhysRevA.38.3098.
[24] C. Lee, W. Yang, R.G. Parr, Development of the colle-salvetti correlation-energy formula into a functional of the electron density, Phys. Rev. B 37 (1988) 785–789, https://doi.org/10.1103/PhysRevB.37.785.
[25] M.J. Frisch, J.A. Pople, J.S. Binkley, Self-consistent molecular orbital methods 25. Supplementary functions for Gaussian basis sets, J. Chem. Phys. 80 (1984) 3265–3269, https://doi.org/10.1063/1.447079.
[26] V.S. Bernales, A.V. Marenich, R. Contreras, C.J. Cramer, D.G. Truhlar, Quantum mechanical continuum solvation models for ionic liquids, J. Phys. Chem. B 116 (2012) 9122–9129, https://doi.org/10.1021/jp304365v.
[27] M. Schmeisser, R. van Eldik, Elucidation of inorganic reaction mechanisms in ionic liquids: The important role of solvent donor and acceptor properties, Dalt. Trans. 43 (2014) 15675–15692, https://doi.org/10.1039/c4dt01239a.
[28] N. Kundu, A. Roy, R. Dutta, N. Sarkar, Translational and Rotational Diffusion of Two Differently Charged Solutes in Ethylammonium Nitrate-Methanol Mixture: Does the Nanostructure of the Amphiphiles Influence the Motion of the Solute?, J Phys. Chem. B 120 (2016) 5481–5490, https://doi.org/10.1021/acs.jpcb.6b02251.
[29] K. Kaneko, Y. Yoshimura, A. Shimizu, Water concentration dependence of the refractive index of various ionic liquid-water mixtures, J. Mol. Liq. 250 (2018) 283–286, https://doi.org/10.1016/j.molliq.2017.12.009.
[30] L. Segade, M. Cabanas, M. Domínguez-Pérez, E. Rilo, S. García-Garabal, M. Turmine, L.M. Varela, V. Gómez-González, B. Docampo-Alvarez, O. Cabeza, Surface and bulk characterisation of mixtures containing alkylammonium nitrates and water or ethanol: Experimental and simulated properties at 298.15 K, J. Mol. Liq. 222 (2016) 663–670, https://doi.org/10.1016/j.molliq.2016.07.107.
[31] A. Nazet, L. Weiß, R. Buchner, Dielectric relaxation of nitromethane and its mixtures with ethylammonium nitrate: Evidence for strong ion association induced by hydrogen bonding, J. Mol. Liq. 228 (2017) 81–90, https://doi.org/10.1016/j.molliq.2016.09.008.
[32] P. Winget, D. M. Dolney, D. J. Giesen, C. J. Cramer, D. G. Truhlar, Minnesota solvent descriptor database for DFT calculation,://comp.chem.umn.edu/solvation/mnsddb.pdf, 1999. Accessed: 2021-12.
[33] H. Montes-Campos, J.M. Otero-Mato, T. Méndez-Morales, E. López-Lago, O. Russina, O. Cabeza, L.J. Gallego, L.M. Varela, Nanostructured solvation in mixtures of protic ionic liquids and long-chained alcohols, J. Chem. Phys. 146 (2017) 124503.
[34] O. Russina, M. Macchiagodena, B. Kirchner, A. Mariani, B. Aoun, M. Russina, R. Caminiti, A. Triolo, Association in ethylammonium nitrate–dimethyl sulfoxide mixtures: First structural and dynamical evidences, J. Non-Cryst. Solids 407 (2015) 333–338.
[35] U. Fatima, H. Montes-Campos, L.M. Varela, et al., Experimental and md simulation investigation on thermophysical properties of binary/ternary mixtures of 1-butyl-3-methylimidazolium trifluoromethanesulfonate with molecular solvents, J. Mol. Liq. 302 (2020) 112481.
[36] T. Méndez-Morales, J. Carrete, O. Cabeza, O. Russina, A. Triolo, L.J. Gallego, L.M. Varela, Solvation of lithium salts in protic ionic liquids: A molecular dynamics study, J. Phys. Chem. B 118 (2014) 761–770, https://doi.org/10.1021/jp410090f.
[37] Y. Shao, K. Shigenobu, M. Watanabe, C. Zhang, Role of viscosity in deviations from the nernst–einstein relation, J. Phys. Chem. B 124 (2020) 4774–4780, https://doi.org/10.1021/acs.jpcb.0c02544.
[38] H.K. Kashyap, H.V.R. Annapureddy, F.O. Raineri, C.J. Margulis, How is charge transport different in ionic liquids and electrolyte solutions?, J Phys. Chem. B 115 (2011) 13212–13221, https://doi.org/10.1021/jp204182c.
[39] L.M. Varela, J. Carrete, M. García, L.J. Gallego, M. Turmine, E. Rilo, O. Cabeza, Pseudolattice theory of charge transport in ionic solutions: Corresponding states law for the electric conductivity, Fluid Phase Equilib. 298 (2010) 280–286, https://doi.org/10.1016/j.fluid.2010.08.013.
[40] H. Montes-Campos, S. Kondrat, E. Rilo, O. Cabeza, L.M. Varela, Random-Alloy Model for the Conductivity of Ionic Liquid-Solvent Mixtures, J. Phys. Chem. C 124 (2020) 11754–11759, https://doi.org/10.1021/acs.jpcc.0c00531.